

# Alkylation of naphthalene with alcohols over acidic mesoporous solids

Ch. Subrahmanyam, B. Viswanathan\*, T.K. Varadarajan

*Department of Chemistry, Indian Institute of Technology, Madras 600 036, India*

Received 6 May 2004; received in revised form 3 August 2004; accepted 30 August 2004

Available online 2 December 2004

## Abstract

Mesoporous cubic MCM-48 was synthesized at a lower concentration of the surfactant. XRD, N<sub>2</sub> adsorption and electron microscopic studies confirmed the formation of cubic phase. Spectroscopic and electron spin resonance techniques confirmed the presence of heteroatom within the framework. The catalytic activities of various acid catalysts have been examined for vapour phase alkylation of naphthalene with alcohols and these studies revealed that aluminium substituted cubic MCM-48 was more active compared to Fe-MCM-48, Al-MCM-41 and H-Y zeolite.

© 2004 Elsevier B.V. All rights reserved.

*Keywords:* Zeolites; Mesoporous MCM-48; Alkylation; Acid catalysis; Naphthalene; Alcohol

## 1. Introduction

In the early nineties, Mobil researchers reported the successful synthesis of mesoporous materials whose pore dimensions are in the range 2–50 nm. The M41S family consists of uni-dimensional hexagonal MCM-41, cubic MCM-48 and lamellar MCM-50 as known members [1]. These materials were prepared through structure-directing agents, which have been proven necessary for the preparation of mesoporous materials. Mesoporous materials possess a periodic framework of regular mesopores, whose dimensions depend mainly on the surfactant chain length. These mesoporous materials possess interesting physical properties that make them potential candidates as catalysts or catalytic supports. Even though M41S series consists of three members, attention has been paid extensively to the synthesis and catalytic exploitation of MCM-41 [2–4]. In this context, many successful attempts have been made to use MCM-41 for the alkylation

of condensed aromatic substrate, naphthalene [5–8]. This is mainly due to the fact that synthesis of MCM-41 requires less severe reaction conditions compared to that of MCM-48. Recent reports on MCM-48, a cubic member of M41S family, suggest that the cubic structure would be suitable for catalytic reactions or catalyst supports [9–11]. On careful observation of the MCM-48 structure it can be seen that the three-dimensional interwoven structure would resist pore blockages. In spite of specific advantages, very little attention has been paid to exploration of the potentials of MCM-48 materials. Till late 1990s this material was synthesized at high concentrations of the surfactant where the surfactant arranges in the liquid crystalline cubic phase [1]. But it would be always desirable to synthesize MCM-48 at low concentrations of the surfactant otherwise calcination for extended period may result in structural collapse of these materials. Keeping this aspect in mind, in this present communication, attempts have been made to synthesize of MCM-48 at lower concentrations of the surfactant. Catalytic functionalities have also been generated by substituting Al and Fe for silicon. Alkylation of naphthalene with alcohols has been carried out as a probe reaction to examine the acid catalytic activity of (Al, Fe)-MCM-48.

\* Corresponding author. Tel.: +91 44 2257 8250; fax: +91 44 2257 8250.

E-mail address: [bviswanathan@hotmail.com](mailto:bviswanathan@hotmail.com) (B. Viswanathan).

## 2. Experimental

### 2.1. Synthesis of Si, Al and Fe substituted MCM-48

MCM-48 materials have been prepared under hydrothermal synthesis conditions using cetyltrimethylammonium bromide (CTAB) as structure-directing template and tetraethyl orthosilicate as the silica source. In a typical synthesis, TEOS was mixed with an aqueous solution of CTAB and to this NaOH in H<sub>2</sub>O and ethanol were added. The homogeneous gel thus obtained was found to have the composition 2 SiO<sub>2</sub>: 0.24 CTAB: 0.5 NaOH: 1–3 EtOH: 195 H<sub>2</sub>O. After ageing at room temperature for 3 h, this homogeneous gel was transferred to a static autoclave and hydrothermally treated under autogeneous pressure at 423 K for 10–15 h. The autoclave was then removed from the oven and cooled to room temperature. After that the solid was recovered by filtration, washed with plenty of water and oven-dried. The powder was then calcined in air at 823 K for 12 h to remove the template [12]. During the calcination, initially, nitrogen atmosphere was maintained in order to preserve the structure. Zeolite Y and H-Al-MCM-41 (Si/Al = 60) were synthesized according to the procedure reported [7,13]. The calcined Na-MCM-48 samples thus obtained were stirred with 1 M ammonium acetate solution at 333 K for 24 h. The solid was then recovered by filtration and washed several times with distilled water to remove the ions present on the extra framework. The same procedure was repeated for three times. The powder was then dried in an oven and calcined in air at 773 K for 6 h to drive off the ammonia gas. Thus, H-MCM-48 samples were obtained.

### 2.2. Characterization

The X-ray diffraction (XRD) patterns were recorded on a D500 Siemens powder diffractometer using monochromatized Cu K $\alpha$  radiation ( $\lambda = 1.5406 \text{ \AA}$ ). Surface area measurements were done by the adsorption–desorption of N<sub>2</sub> at 77 K using a Sorptomatic 1990 (Carlo Erba) instrument. Samples before the measurements were outgassed at 423 K for 12 h to remove the physisorbed gases. Acidic sites were identified through temperature programmed desorption of ammonia. Temperature programmed desorption of ammonia serves as a dependable technique for the quantitative determination of the acid strength distribution. In TPD studies, palletized catalyst (100 mg) was activated at 473 K inside the reactor under a helium flow (50 ml/min) for half an hour. After cooling to room temperature, a current of ammonia was passed through the catalyst and the system was allowed to attain equilibrium. Helium was used to flush out the excess and physisorbed ammonia. The temperature was then raised in a stepwise manner at a linear heating rate of about 20 K/min. The ammonia desorbed from 373 to 873 K at intervals of 50 K was then trapped in dilute sulphuric acid and estimated volumetrically by back titration with standard NaOH. UV–vis spectra were recorded on a Perkin-Elmer (Model 1760) spectrophotometer whereas ESR-spectra were recorded on a Varian-115

spectrometer. HR-TEM measurements were carried out on a Philips CM300UT FEG with a 300 kV field emission gun. Thermal analyses of the samples were made with a thermal analyzer (Perkin-Elmer model TGA 7) at a heating rate of 20 K/min.

### 2.3. Catalytic activity

The catalytic activities of Al-MCM-48 and Fe-MCM-48 were tested for the vapour phase alkylation of naphthalene with *n*-propyl alcohol and *n*-butyl alcohol as alkylating agents. Vapour phase alkylation of naphthalene was performed in a fixed bed Pyrex flow reactor working at atmospheric pressure. The reactants were fed into the reactor by a motor-driven syringe infusion system. The feed rate was maintained accurately by proper calibration from time to time. For vapour phase reaction, about 0.5 g of the catalyst was used for each run. Products collected for the first 20 min were discarded to ensure the attainment of the steady state. The products coming out of the reactor in the vapour phase were cooled by means of a double-walled Liebig condenser and liquid products were collected in a cold trap maintained at the temperature of freezing mixture (ice + NaCl). The catalysts were regenerated after each run by passing air at 723 K for 6 h. Identification of the product was done with GC–MS whereas quantitative analysis of the product was done with a Nucon gas chromatograph.

## 3. Results and discussion

### 3.1. Powder X-ray diffraction study of H-MCM-48

The low angle X-ray diffraction patterns of the MCM-48 samples (Si, Al, Fe)-MCM-48 are given in Figs. 1 and 2. The diffraction pattern consists of peaks corresponding to the reflections that are characteristic of cubic MCM-48 lattice

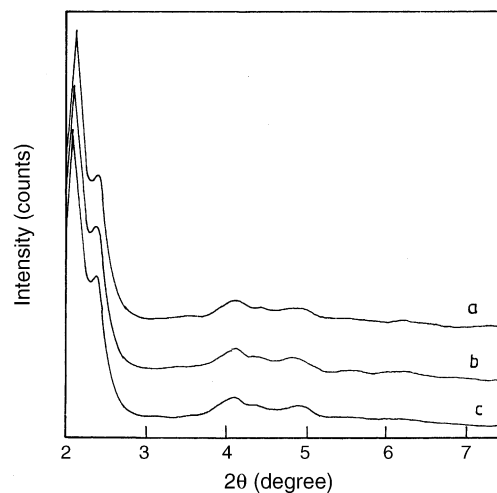


Fig. 1. XRD patterns of as-synthesized materials: (a) Si-MCM-48, (b) Al-MCM-48 and (c) Fe-MCM-48.

Table 1  
XRD data of Si, Al and Fe-MCM-48 catalysts

Catalyst	$d_{211}$ (uncalculated) (Å)	$d_{211}$ (calculated) (Å)	$a = d_{211}\sqrt{h^2 + k^2 + l^2}$ (Å)
Si-MCM-48	33.7	32.9	80.5
Al-MCM-48	33.69	32.75	80.22
Fe-MCM-48	34.75	33.1	81.07

similar to the one reported by Beck et al. [1]. This XRD pattern is characteristic of the material with semi crystalline nature. The XRD data along with cell parameter values are given in Table 1 from which it is clear that with the incorporation of heteroatom in the framework, the cell parameter value increases slightly. Even though this cannot be taken into account for the incorporation of subsequent atoms in the framework, it provides first hand information regarding the presence of heteroatom.

It is well known that higher loadings of metal atoms result in the formation of extra framework oxides. Keeping this aspect in mind, in the present study, incorporation of the Al and Fe was restricted only to Al/M = 150. Calcination of the as-synthesized MCM-48 (Fig. 2) did not result in collapse of the structure and in addition, the sample maintains the same XRD pattern with almost the same intensity indicating that the sample maintains the same morphology even after calcination. However, a slight decrease in the  $d_{211}$  spacing was observed indicating contraction of the structure during calcination.

It was observed that addition of ethanol plays an important role as it directs the final structure. The role of ethanol is probably to stimulate the transformation of MCM-41 to MCM-48 by allowing the proper condensation of silanol groups. To emphasize this point, the same procedure was adopted without adding ethanol, which resulted in the MCM-41 type material only. Fig. 3a and b represents the XRD patterns of the materials synthesized in the presence and absence of ethanol,

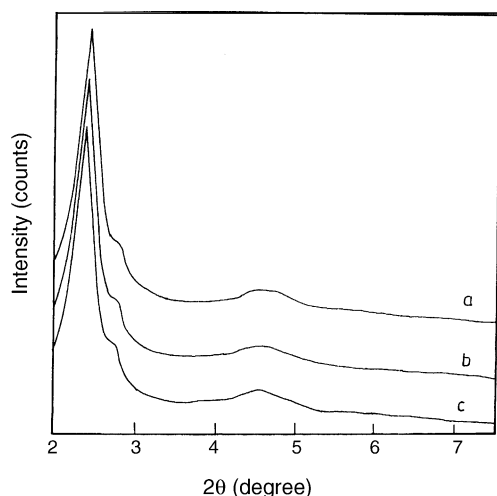


Fig. 2. XRD patterns of calcined materials: (a) Si-MCM-48, (b) Al-MCM-48 and (c) Fe-MCM-48.

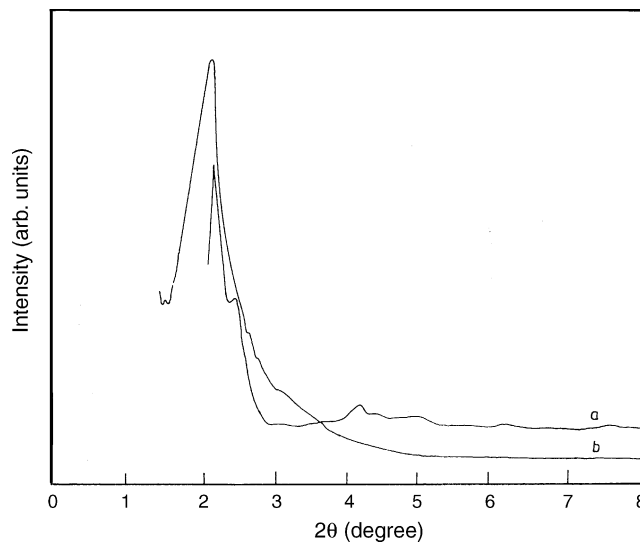


Fig. 3. XRD patterns of Si-MCM-48 (a) in the presence of ethanol and (b) in the absence of ethanol.

respectively. Ethanol thus facilitates the condensation process and directs the cubic interwoven structure.

### 3.2. $N_2$ adsorption–desorption isotherms

$N_2$  adsorption–desorption isotherms of calcined Si-MCM-48, Al-MCM-48 and Fe-MCM-48 are shown in Fig. 4. A typical type IV isotherm with a hysteresis loop was observed, which is characteristic of mesoporous solids. The observed isotherm can be explained as follows: adsorption at lower relative pressures ( $p/p_0$ ) is due to the formation of monolayer of nitrogen molecules on the walls of mesoporous MCM-48, which is followed by a sharp inflection due to the capillary condensation within the mesopores [1]. The BET surface areas of the studied catalysts are given in Table 2.

### 3.3. Thermogravimetric analysis (TGA)

The thermograms of the Si, Al and Fe incorporated MCM-48 materials are shown in Fig. 5. Thermograms of the

Table 2  
 $N_2$  adsorption data of Si, Al and Fe-MCM-48 catalysts

Catalyst	BET surface area ( $m^2/g$ )	Pore size (Å)	Pore volume ( $cc/g$ )
Si-MCM-48	1020	28	1.01
Al-MCM-48	975	28.5	0.95
Fe-MCM-48	840	28	0.91

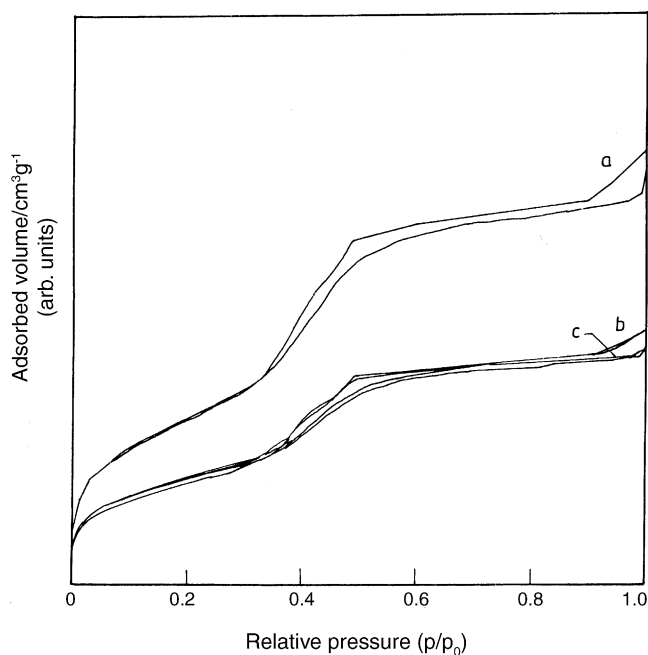


Fig. 4.  $N_2$  adsorption–desorption isotherms of (a) Si-MCM-48, (b) Al-MCM-48 and (c) Fe-MCM-48.

as-synthesized catalyst revealed different nature of interactions of the surfactant molecules with the framework species. In the case of siliceous MCM-48 catalysts, weight loss is observed in a three-step decomposition process. In the first step, the observed weight loss around 373 K is mainly due to the water, which is adsorbed on the catalyst surface. The second and main weight loss observed in the temperature range 423–623 K is due to the removal of the template, which is occluded in the mesopores. The final weight loss above 623 K is due to the removal of the water due to the condensation of silanol groups. A similar trend was also ob-

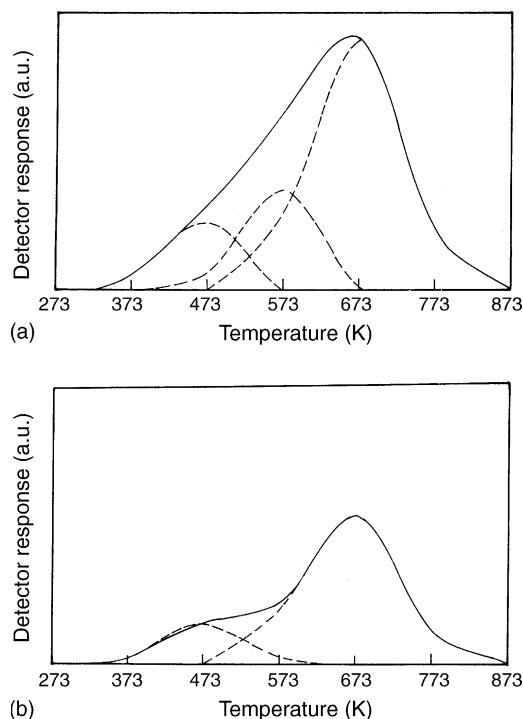


Fig. 6. TPDA profiles of (a) Al-MCM-48 and (b) Fe-MCM-48.

served in the case of Al- and Fe-substituted materials. Significant difference in the behavior of thermogram was not observed, as the amount of heteroatom is very small in all the cases.

#### 3.4. Temperature programmed desorption studies (TPD)

TPD profiles of the acid catalysts are shown in Fig. 6. TPD pattern of Al-MCM-48 shows the presence of three different types of acid sites. The sites present in the low

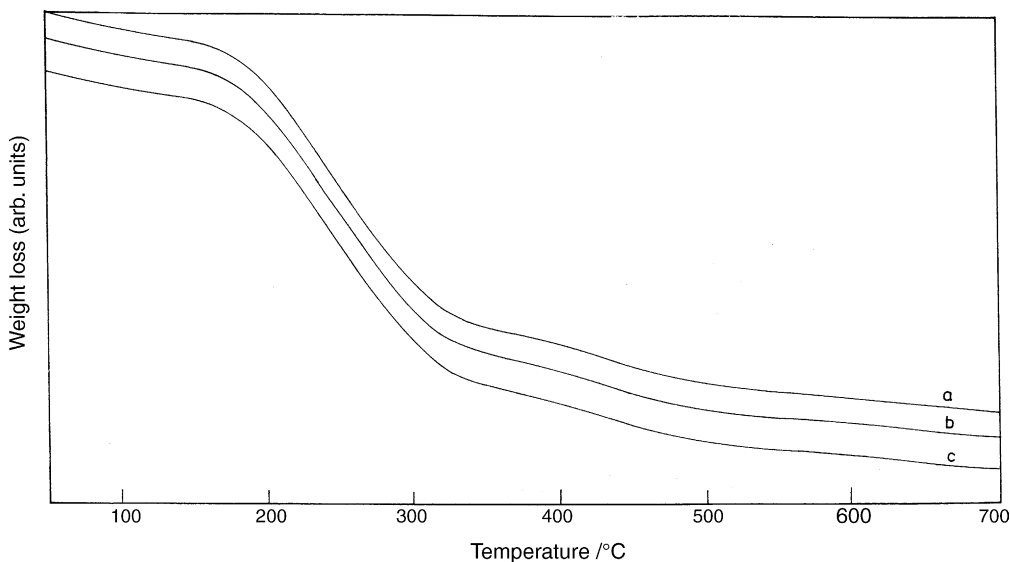


Fig. 5. TGA patterns of (a) Si-MCM-48, (b) Al-MCM-48 and (c) Fe-MCM-48.

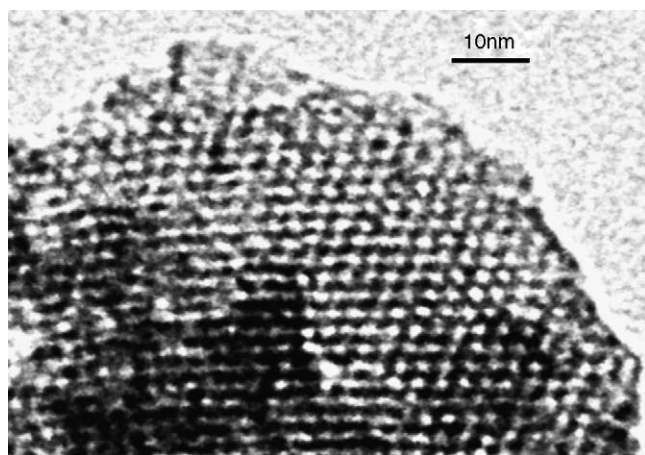


Fig. 7. HR-TEM of Si-MCM-48.

temperature region are due to the desorption of ammonia from weakly acidic sites. With increase in temperature, evolution of ammonia from relatively strong physisorbed sites is observed [14]. H-Fe-MCM-48 shows two types of acidic sites. The sites present in the low temperature region are due to ammonia desorbed from weakly acidic sites, followed by a broad distribution of moderately acidic sites at higher temperature.

### 3.5. Transmission electron microscopic study (TEM)

In the case of porous solids, transmission electron microscopic study provides information regarding the surface morphology and pore structure. The TEM image of MCM-48 (Fig. 7) confirms the mesoporous nature of the catalyst synthesized and also supports the pore size data obtained from N<sub>2</sub> adsorption. In addition, transmission electron micrographs provide information regarding the arrangement of the pores. From the figures, it is clear that the material formed in the present study possesses regular channels arranged in three dimensions.

### 3.6. UV–vis (Nujol) spectral studies

UV–vis spectra of as-synthesized and calcined mesoporous Fe-MCM-48, which are recorded in the Nujol mode, are given in Fig. 8. As-synthesized Fe-MCM-48 shows a band around 240 nm, which is also observed in calcined samples. Based on the earlier reports, this band is assigned to the ligand-to-metal charge transfer transition, indicating the presence of isolated FeO<sub>4</sub><sup>−</sup> type species. Interestingly, in both uncalcined and calcined samples, the bands corresponding to d–d transitions are absent indicating the absence of extraframework bulk Fe<sub>2</sub>O<sub>3</sub> species. On calcination, the band observed around 240 nm was retained indicating the presence of iron in the framework of calcined sample. In addition, absence of bands in the visible region rules out the presence of extraframework oxide species [15–17].

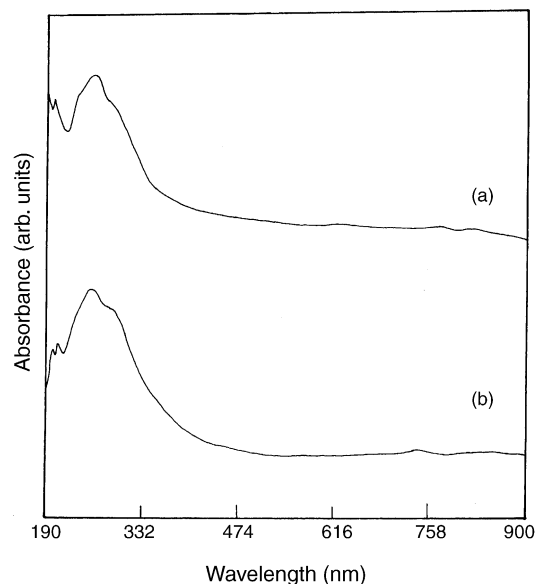


Fig. 8. UV–vis spectra of Fe-MCM-48: (a) as-synthesized and (b) calcined.

### 3.7. Electron spin resonance study (ESR)

Since ferric iron is paramagnetic in both low-spin and high-spin electronic configurations, ESR spectroscopy should be a method for characterizing the iron sites in zeolites and related materials like aluminophosphates. However, in the case of iron substituted materials, the interpretation of the ESR spectra is difficult due to complications associated with the homogeneous broadening, which arises from the zero field splitting and overlapping signals. However, in the literature, observed signals at  $g = 4.3$ , 2.0 and 2.02 were assigned to the presence of iron in distorted tetrahedral, framework tetrahedral and octahedral environments, respectively [15–17]. In the present study, the X-band ESR spectrum (Fig. 9) consists of major signals at  $g = 4.3$  and 2.0. These signals have been assigned to the framework tetrahedral iron, extra framework octahedral iron oxide phases, respectively. This assignment is also in accordance with the earlier observations.

### 3.8. Propylation of naphthalene

This reaction is chosen to test the acid catalytic activity of these catalysts in the temperature range 598–678 K. The activities obtained are compared with that obtained on H-Y and H-Al-MCM-41. This temperature range would be ideal for testing the stability of the synthesized catalysts, as it is known that these systems are not stable at higher temperatures.

Data on the catalytic activity of *n*-propylation of naphthalene at various flow rates in the studied temperature range are given in Tables 3 and 4. At a given feed rate, it was observed that the conversion of naphthalene decreases with increase in temperature. This decrease is predominant over H-Y zeolite when compared to mesoporous solids.

Table 3  
Propylation of naphthalene over acid catalysts

Catalyst	Temperature (K)	Conversion (%)	Product selectivity (%)		
			$\beta$ -Isopropyl naphthalene	$\beta$ - <i>n</i> -Propyl naphthalene	Di-substituted naphthalene
H-Y	598	28.6	78.0	–	22.0
H-Al-MCM-41	598	33.2	82.0	13.0	5.0
H-Al-MCM-48	598	34.1	84.1	9.5	6.4
H-Fe-MCM-48	598	32.8	71.9	22.1	–
HY	623	17.3	88.0	–	12.0
H-Al-MCM-41	623	30.5	83.5	13.0	3.5
H-Al-MCM-48	623	30.5	85.0	10.0	5.0
H-Fe-MCM-48	623	29.4	72.5	27.5	–
HY	648	12.5	>99	–	–
H-Al-MCM-41	648	30.5	83.5	13.0	3.5
H-Al-MCM-48	648	34.5	87.0	6.6	6.4
H-Fe-MCM-48	648	28.5	84.7	15.1	Traces
HY	673	7.4	>99	–	–
H-Al-MCM-41	673	18.7	96.0	–	4.0
H-Al-MCM-48	673	19.4	92.0	–	8.0
H-Fe-MCM-48	673	14.6	>99	Traces	–

Reaction conditions: weight of the catalyst = 500 mg and flow rate = 10 ml/h. Naphthalene:alcohol = 1:100 (mole ratio).

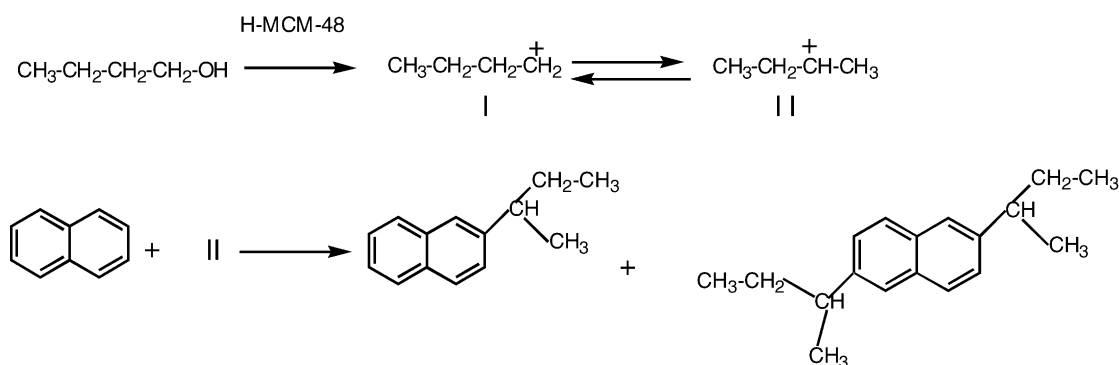
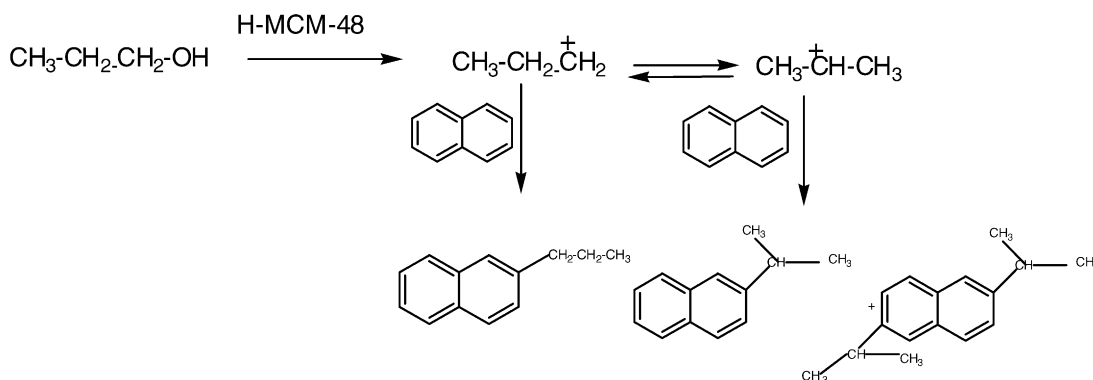
The *n*-propylation of naphthalene proceeds simultaneously by several mechanisms. The selectivity is determined by all these routes as well as by the molecular sieving effects, when the catalysts employed are porous in nature. In the case of the *n*-propylation of naphthalene both  $\alpha$  and  $\beta$  positions are likely to be alkylated [18]. Kinetic factors favour alkylation at the  $\alpha$  position where as thermodynamic factors favor at the  $\beta$  position. Even though, at initial stages, alkylation takes place on the  $\alpha$  site, due to the peri interactions, the  $\alpha$  product will be destabilized and thereby results in more stable  $\beta$  alkylated naphthalene. Under the reaction conditions employed in the present study, mainly monosubstituted products are formed over Al-MCM-48 and Fe-MCM-48. However, a little amount of 2,6-disubstituted products are also observed.

When the reactant molecules diffuse through the pores of the molecular sieves, there is a preferential adsorption of *n*-propyl alcohol over naphthalene on the acid sites of the catalysts thereby resulting in the formation of primary carbocation. As primary carbocation is relatively unstable, it isomerizes on strong acid sites to give a stable secondary carbocation. The formation of  $\beta$ -isopropyl naphthalene is a result of the attack of stable secondary carbocation at the  $\beta$  position of the ring, where as the formation of  $\beta$ -*n*-propyl naphthalene is due to the attack of the primary carbocation on the  $\beta$  position of the ring. This alkylation of naphthalene by these carbocations will follow the Friedel-Crafts mechanism, which is given in Scheme 1. Among the catalysts employed, H-Al-MCM-48 shows higher activity when

Table 4  
Propylation of naphthalene over acid catalysts

Catalyst	Temperature (K)	Conversion (%)	Product selectivity (%)		
			$\beta$ -Isopropyl naphthalene	$\beta$ - <i>n</i> -Propyl naphthalene	Di-substituted naphthalene
H-Y	598	34.6	80.0	–	–
H-Al-MCM-41	598	35.8	84.5	15.1	Traces
H-Al-MCM-48	598	37.5	83.5	12.8	3.7
H-Fe-MCM-48	598	34.0	87.1	12.9	–
H-Y	623	20.2	90.0	–	10.0
H-Al-MCM-41	623	31.3	88.5	11.4	Traces
H-Al-MCM-48	623	32.7	87.0	10.5	2.5
H-Fe-MCM-48	623	29.9	90.1	9.9	–
H-Y	648	15.0	95.0	–	4.7
H-Al-MCM-41	648	27.4	90.0	9.8	Traces
H-Al-MCM-48	648	27.4	87.5	11.5	1.0
H-Fe-MCM-48	648	25.6	91.1	8.9	–
H-Y	648	9.2	98.0	–	Traces
H-Al-MCM-41	673	24.0	89.1	10.2	Traces
H-Al-MCM-48	673	24.7	90.2	9.5	Traces
H-Fe-MCM-48	673	22.9	87.1	12.9	–

Reaction conditions: weight of the catalyst = 500 mg and flow rate = 12.5 ml/h. Naphthalene:alcohol = 1:100(mole ratio).



compared to H-Al-MCM-41. This is due to the fact that H-Al-MCM-48 will impose less diffusional constraints for the diffusion of the products. Since MCM-48 has a three-dimensional channel system, it will allow the products to diffuse easily through its channels. Among MCM-48 catalysts, the difference in the observed higher activities can be attributed to the difference in acidic nature.

At higher temperatures, conversion of naphthalene is lower because the oligomerisation reaction is preferred on stronger acid sites of H-Y zeolites compared to other mesoporous solids. Thus, the conversion with respect to naphthalene is low over these zeolite catalysts. However, the observed activity is due to the presence of stronger acid sites on the surface of H-Y zeolite [7,8]. Another interesting feature is the formation of *n*-propyl naphthalene on mesoporous catalysts. This observation can be explained based on the less strong acidity of mesoporous solids, which facilitates the stabilization of *n*-propyl carbocation. Since the isomerization of *n*-propyl to secondary propyl carbocation demands strong acid sites, its complete conversion might not be possible on the surface of mesoporous solid. When the flow rate of the reactants is increased, the conversion of naphthalene is found to increase on all the catalysts studied. This is due to the fact that when the flow rate is lower, the reactants will be in contact with the acid sites for a longer time, resulting in the oligomerization reaction. After the reaction, catalyst was regenerated

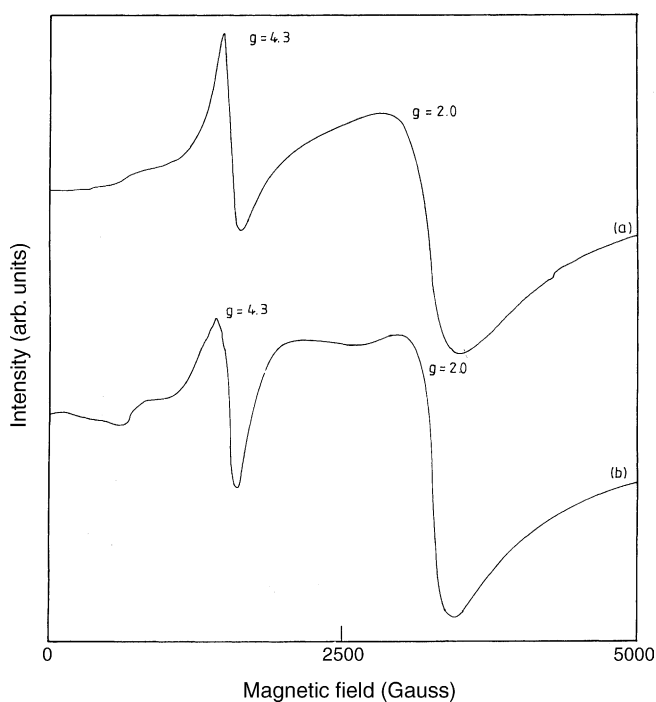


Fig. 9. ESR spectra of Fe-MCM-48 (a) as-synthesized (b) calcined.

Table 5  
Butylation of naphthalene over acid catalysts

Catalyst	Temperature (K)	Conversion (%)	Product selectivity (%)	
			$\beta$ -Isobutyl naphthalene	Di-substituted naphthalene
H-Y	598	0.0	–	–
H-Al-MCM-41	598	5.4	>99	Traces
H-Al-MCM-48	598	5.4	95	5.0
H-Fe-MCM-48	598	4.9	>99	–
H-Al-MCM-41	623	5.5	>99	–
H-Al-MCM-48	623	5.7	91.2	8.8
H-Fe-MCM-48	623	5.2	>99	–
H-Al-MCM-41	648	5.5	>99	–
H-Al-MCM-48	648	6.4	92.0	8.0
H-Fe-MCM-48	648	5.1	>99	–
H-Al-MCM-41	673	5.0	>99	–
H-Al-MCM-48	673	5.8	92.8	7.2
H-Fe-MCM-48	673	4.3	>99	–

Reaction conditions: weight of the catalyst = 500 mg and flow rate = 10 ml/h. Naphthalene:alcohol = 1:100 (mole ratio).

Table 6  
Butylation of naphthalene over acid catalysts

Catalyst	Temperature (K)	Conversion (%)	Product selectivity (%)	
			$\beta$ -Isobutyl naphthalene	Di-substituted naphthalene
H-Al-MCM-41	598	5.0	>99	–
H-Al-MCM-48	598	5.4	95	5.0
H-Fe-MCM-48	598	4.5	>99	–
H-Al-MCM-41	623	5.6	>99	–
H-Al-MCM-48	623	6.0	97	3.0
H-Fe-MCM-48	623	5.2	>99	–
H-Al-MCM-41	648	5.0	>99	–
H-Al-MCM-48	648	5.0	99	Traces
H-Fe-MCM-48	648	4.8	>99	–
H-Al-MCM-41	673	4.8	>99	–
H-Al-MCM-48	673	5.0	>99	–
H-Fe-MCM-48	673	4.5	>99	–

Reaction conditions: weight of the catalyst = 500 mg and flow rate = 12.5 ml/h. Naphthalene:alcohol = 1:100 (mole ratio).

and reused for subsequent cycles. The loss of activity was negligible.

### 3.9. Butylation of naphthalene

The results on the *n*-butylation of naphthalene in the temperature range 598–673 K at different flow rates are given in Tables 5 and 6. The conversion observed for *n*-butylation of naphthalene reaction is lower when compared to *n*-propylation. It is also interesting to note that *n*-butyl derivative of naphthalene is not observed over H-Al-MCM-48 and H-Fe-MCM-48. This is because *n*-butyl carbocation is unstable and it readily isomerizes to stable secondary carbocation, although this isomerization step depends on the strength of the acid sites. Among the mesoporous catalysts, H-Al-MCM-48 is more active when compared to its iron substituted cubic analogue. The possible reaction mechanism is given in Scheme 2.

## 4. Conclusions

Mesoporous cubic MCM-48 has been synthesized at a lower concentration of the surfactant. Various characterization techniques confirm the formation of cubic phase and also the presence of the heteroatom within the framework. Acidic functionalities have been generated with incorporation of trivalent aluminium and iron. Alkylation of naphthalene with alcohols over these systems indicates that MCM-48 exhibits higher conversion when compared to one-dimensional counterpart, MCM-41. Among Al and Fe incorporated MCM-48, the former is more active.

## Acknowledgements

We would like to thank Dr. M.R.K. Prasad, Dr. Suja, Dr. Benoit Louis and Dr. Ch. Patra for their help in characterizing catalysts.

## References

- [1] J.S. Beck, J.C. Vartuli, W.J. Roth, M.E. Leonowicz, C.T. Kresge, K.D. Schmitt, C.T.W. Chu, D.H. Olson, E.W. Sheppard, S.B. McCullen, J.B. Higgins, J.L. Schlenker, *J. Am. Chem. Soc.* 114 (1992) 10834.
- [2] A. Corma, *Chem. Rev.* 97 (1994) 2373.
- [3] A. Corma, V. Fornes, M.T. Navarro, J. Perez-Pariente, *J. Catal.* 148 (1994) 569–574.
- [4] A. Corma, M.T. Navarro, J. Perez, Pariente, *Chem. Commun.* (1994) 147.
- [5] G. Kamalakar, M.R.K. Prasad, S.J. Kulkarni, S. Narayanan, K.V. Raghavan, *Micro. Meso. Mater.* 38 (2000) 135.
- [6] G. Kamalakar, M.R.K. Prasad, S.J. Kulkarni, K.V. Raghavan, *Micro. Meso. Mater.* 52 (2002) 151.
- [7] B. Chakraborty, A.C. Pulikottil, B. Viswanthan, *Catal. Lett.* 39 (1996) 63.
- [8] E. Armengol, M.L. Cano, A. Corma, H. Garcia, M.T. Navarro, *J. Chem. Soc. Chem. Commun.* (1995) 519.
- [9] K.A. Koyano, T. Tatsumi, *Chem. Commun.* (1996) 145–146.
- [10] M. Mathieu, P. van Der Voort, B.M. Weckhuysen, R.R. Rao, G. Catana, R.A. Schoonheydt, E.F. Vansant, *J. Phy. Chem B* 105 (2001) 3393.
- [11] K.A. Koyano, T. Tatsumi, *Stud. Surf. Sci. Catal.* 105A (1997) 93.
- [12] Ch. Subrahmanyam, B. Louis, F. Rainone, B. Viswanthan, A. Renken, T.K. Varadarajan, *Appl. Catal. A: General* 241 (2003) 205.
- [13] B Chakraborty, (1998) Ph.D thesis, IIT Madras.
- [14] M. Niwa, N. Katada, *Catal. Sur. Jap.* 1 (1997) 215.
- [15] D. Goldfrab, M. Bernardo, K.G. Strohmaier, D.E.W. Vaughan, H. Thomann, *B. J. Am. Chem. Soc.* 116 (1994) 6344.
- [16] J. Das, C.V.V. Satyanarayana, D.K. Chakraborty, S.N. Piramanayagam, S.N. Shringi, *J. Chem. Soc. Far. Tran.* 88 (1992) 3255.
- [17] S.K. Mohapatra, S.B. Sahoo, W. Keune, P. Selvam, *Chem. Commun.* (2002) 1466.
- [18] G.A. Olah, *Friedel Crafts and Related Reactions Part I, vol. II*, Interscience, New York, 1964.